Appl Phys A (2009) 96: 5–10
DOI 10.1007/s00339-009-5177-3

Applied Physics A
Materials Science & Processing

Quantum dynamical study of the amplitude collapse and revival of coherent A_{1g} phonons in bismuth: a classical phenomenon?

Momar S. Diakhate · Eeuwe S. Zijlstra · Martin E. Garcia

Received: 19 November 2008 / Accepted: 27 February 2009 / Published online: 10 March 2009

Abstract We parameterize the potential energy surface of bismuth after intense laser excitation using accurate full-potential linearized augmented plane wave calculations. Anharmonic contributions up to the fifth power in the A_{1g} phonon coordinate are given as a function of the absorbed laser energy. Using a previously described model including effects of electron–phonon coupling and carrier diffusion due to Johnson et al., we obtain the time-dependent potential energy surface for any given laser pulse shape and duration. On the basis of this parameterization we perform quantum dynamical simulations to study the experimentally observed amplitude collapse and revival of coherent A_{1g} phonons in bismuth considering work of Misochko et al. Our results strongly indicate that the observed beatings are not related to quantum effects and are most probably of classical origin.

PACS 63.20.Ry · 78.47.J-

1 Introduction

When an intense femtosecond laser pulse interacts with a semiconductor in such a way that a considerable fraction of the valence electrons is excited, the interatomic potential, or potential energy surface can change dramatically. As a consequence, the solid can undergo ultrafast phase transitions, or, as a precursor to laser-induced structural changes, large amplitude coherent phonons can be excited [1]. These collective lattice vibrations, which usually involve only a few degrees of freedom, provide a useful system to study both laser–matter interactions and the physical processes related to the relaxation of the nonthermal state induced by the laser [2–4]. A question that has received relatively little attention is, whether the induced phonons behave classically as is usually assumed or whether some quantum effects may be detected [5]. An in this respect interesting observation has recently been made by Misochko et al. [6] in bismuth: it was found that the amplitude of coherent A_{1g} phonon oscillations vanishes and, at a later time, reappears when the fluence of the pump laser is above a certain threshold value. This phenomenon, which was explained as a quantum mechanical effect and was therefore referred to as "amplitude collapse and revival" (see Sect. 3), is the main topic of this paper. In particular, our goal is to clarify whether its origin is classical or quantum mechanical. To this aim we have performed quantum dynamical simulations on time-dependent potential energy surfaces, which we describe in Sect. 5. Because we expect that our potential energy surfaces will also be useful for the simulation and interpretation of other experiments, we describe its derivation and parameterization in detail in Sect. 4. A brief explanation of "amplitude collapse and revival" is given in Sect. 3. In Sect. 2 we provide a short description of the atomic structure of bismuth.

2 Peierls distortion

The atoms in bismuth are located on positions near the vertices of a distorted simple cubic lattice. For a detailed description of the atomic structure of bismuth we refer the interested reader to [7]. Here the most relevant point is that the bismuth unit cell is doubled as compared to the distorted

M.S. Diakhate · E.S. Zijlstra (✉) · M.E. Garcia
Theoretische Physik, Universität Kassel, Heinrich-Plett-Str. 40, 34132 Kassel, Germany
e-mail: zijlstra@physik.uni-kassel.de

M.E. Garcia
e-mail: magarcia@physik.uni-kassel.de

simple cubic lattice due to a Peierls instability. The magnitude of the Peierls displacement can be derived from the atomic coordinate z, which is usually expressed as a fraction of the lattice parameter $c = 11.8$ Å. A value of $z = 0.25$ indicates no Peierls distortion. In the ground state $z = 0.234$, which means that atomic planes are displaced by 0.19 Å in alternating directions. The coordinate z is perhaps the most important parameter in the rest of this paper, because it is associated to the A_{1g} phonons. These phonons can be excited by a femtosecond laser pulse and can, for example, be detected through induced changes in the isotropic reflectivity. As we will see below, the A_{1g} phonon frequency is proportional to the second derivative of the potential energy curve along the z direction.

3 Theory of amplitude collapse and revival

A theoretical derivation of the amplitude collapse and revival of wave packets in weakly anharmonic potentials has been given in [8]. Here we just mention the main results. (i) Wave packets in a harmonic potential move along classical trajectories. They typically spread, but the spreading is reversible. After one period a packet completely regains its initial shape due to the equidistant character of the spectrum of states. (ii) Anharmonicity leads to a quantum dephasing of a wave packet. The time scale on which this happens can be estimated from

$$T_{\mathrm{rev}} = \frac{2T_{\mathrm{cl}}}{h|\frac{\partial \nu_{\mathrm{cl}}}{\partial E}|}. \tag{1}$$

Here, T_{cl} is the classical period of the trajectory, ν_{cl} is the classical frequency, and E is the expectation value of the energy of the wave packet. Note, that all quantities appearing on the right-hand side of (1) are classical. For times $t \ll T_{\mathrm{rev}}$, the wave packet behaves essentially classically. (iii) If the anharmonicity is small, the quantum dephasing is reversible. In particular, at $t = T_{\mathrm{rev}}$ the initial wave packet is approximately restored (this is called revival) and at $t = T_{\mathrm{rev}}/2$ the wave packet is shifted by half a classical period (the so-called revival of order 1/2). (iv) In between these revivals, which are phase shifted with respect to each other, the expectation value of the amplitude of the oscillation disappears. This is sometimes referred to as "amplitude collapse of the wave packet".

The derivation given in [8] relies on the discrete nature of the spectrum of states. Therefore, it should be expected that "amplitude collapse and revival" can only be observed in finite systems. In (1) this becomes apparent if one realizes that ν_{cl} is an intrinsic quantity, which changes little with system size, and that E is an extrinsic quantity, which scales roughly linearly with, for example, the number of atoms in a molecule.

Experimentally, amplitude collapse and revival has unambiguously been observed for electronic wave packets in Rydberg atoms [9] and for molecular wave packets in small molecules [10]. In addition, the recent experiment on bulk bismuth that we have mentioned in the introduction has also been explained in the same way. However, a theoretical justification for the conclusion of [6], that the A_{1g} phonons in solid Bi behave quantum mechanically is lacking, as we will point out below.

4 Potential energy surface

4.1 Selfconsistent full-potential linearized augmented plane wave calculations

We computed the total energy of bismuth with the all-electron full-potential linearized augmented plane wave (LAPW) computer program WIEN2k [11]. This implementation of density functional theory (DFT) [12, 13] has been designed to provide accurate results, which validity depends on no other approximation than the local density approximation [14]. Details of our calculations are as follows. In our basis set we included LAPW's with energies up to 18.9 Ry. Atomic spheres around the Bi atoms had radii of 2.3 a_0. Inside the atomic spheres we used a combination of augmented plane waves and local orbitals (APW + lo) [15, 16] to describe the 5*d*, 6*s*, and 6*p* states. The augmentation energies for these APW + lo's were −1.237, −0.274, and 0.262 Ry, respectively. In order to achieve a further reduction of linearization errors we employed additional 6*p* and 6*d* local orbitals [17] with energy parameters of 2.262 and 0.142 Ry, respectively. We treated spin–orbit coupling selfconsistently in a second variational procedure [18], where we used the scalar relativistic eigenstates up to 10 Ry as a basis for the relativistic calculation. We sampled the entire Brillouin zone with 32768k points using temperature smearing ($T_e = 1$ mRy). The above parameters make our present computations substantially more accurate than the DFT results that we have previously published on bismuth [7].

4.2 Effect of laser excitation

To describe bismuth after laser excitation we have used the following physical picture: The laser pulse creates electrons and holes, which undergo dephasing and collisions on a time scale that is much shorter than the typical time of ionic motion (∼300 fs, based on the A_{1g} phonon frequency). Therefore one can for all practical purposes assume that the excited carriers thermalize instantaneously. In other words, we simulated the effect of the excitation by an ultrashort laser pulse by heating the electrons. In our calculations the electronic temperature T_e ranged between 1 mRy for the electronic ground state and 28 mRy (4.4×10^3 K) for the highest

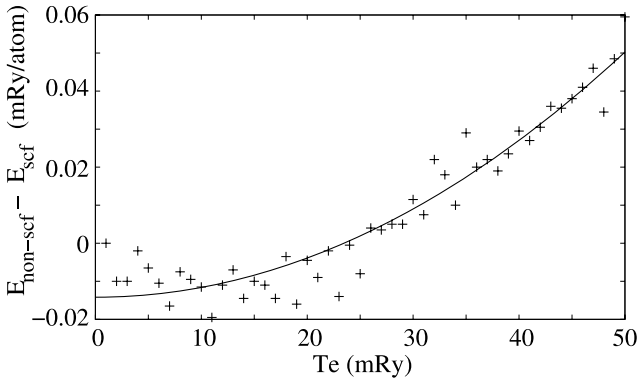

Fig. 1 Difference of the total energies for finite electronic temperatures using (i) (2) (non-selfconsistent approach) and (ii) standard temperature-dependent DFT (selfconsistent approach). The data shown are for $z = 0.2341$. The *solid line* is a guide to the eye, showing the trend of the data

excited state. Here we wish to mention, that we have used the microcanonical ensemble for the electrons (there is no heat bath). This means that the electronic entropy S_e, not the temperature T_e, was a constant of motion. The atomic z coordinate of bismuth was treated as an external parameter.

In practical computations, we have calculated the total energies at elevated electronic temperatures T_e (corresponding to constant values of the entropy S_e) using

$$E_{\mathrm{tot}}(T_e) = E_{\mathrm{tot}}(\mathrm{gs}) + \Delta E_{\mathrm{band}}, \tag{2}$$

where $E_{\mathrm{tot}}(\mathrm{gs})$ is the selfconsistent total energy of the electronic ground state (see Sect. 4.1) and $\Delta E_{\mathrm{band}} = E_{\mathrm{band}}(T_e) - E_{\mathrm{band}}(\mathrm{gs})$. This approach is based on the interpretation of the Kohn–Sham energies [13] as single-electron excitation energies. In standard temperature-dependent DFT [19] the electronic occupation numbers are incorporated in the self-consistent cycle to take into account possible screening effects. We have also performed such calculations, assuming that the local density approximation of [14] is still valid at high temperatures. We found that the differences between the predictions of both approaches are very small, typically less than 0.02 mRy/atom for $T_e \leq 28$ mRy. This is illustrated in Fig. 1 for $z = 0.2341$.

4.3 Parameterization

We fitted our total energies, which we computed on a fine grid of z values ($z = 0.2250, 0.2251, \ldots, 0.2480$) and for 28 different electronic entropies (the entropies were chosen in such a way that $T_e = 1, 2, \ldots, 28$ mRy at $z = 0.2341$) to a function of the form

$$V(z, E_0) = E_0 + 4373.0\nu^2(z - z_{\mathrm{eq}})^2 + \gamma(z - z_{\mathrm{eq}})^3 + \delta(z - z_{\mathrm{eq}})^4 + \epsilon(z - z_{\mathrm{eq}})^5, \tag{3}$$

where E_0 was entropy dependent (a different value has been allowed for each electronic entropy) and the parameters ν, z_{eq}, γ, δ, and ϵ depended implicitly on the electronic entropy through E_0 via the following relations:

$$\nu = \nu_0 + \nu_1 E_0 + \nu_2 E_0^2 + \nu_3 E_0^3 + \nu_4 E_0^4 + \nu_5 E_0^5, \tag{4}$$

$$z_{\mathrm{eq}} = z_0 + z_1 E_0 + z_2 E_0^2 + z_3 E_0^3, \tag{5}$$

$$\gamma = \gamma_0 + \gamma_{1/2} E_0^{1/2} + \gamma_{3/2} E_0^{3/2}, \tag{6}$$

$$\delta = \delta_0 + \delta_1 E_0 + \delta_2 E_0^2 + \delta_3 E_0^3, \tag{7}$$

$$\epsilon = \epsilon_0 + \epsilon_{1/2} E_0^{1/2} + \epsilon_1 E_0, \tag{8}$$

where E_0 was shifted by a constant to make it zero for the electronic ground state calculation. The symbols in the above equations have the following physical meaning and units: ν is the harmonic A_{1g} phonon frequency in THz, $V(z, E_0)$ is the total energy in mRy/atom, and z_{eq} is the quasi-equilibrium value of the atomic z coordinate of Bi (see Sect. 2). γ, δ, and ϵ describe the third, fourth, and fifth order anharmonicity of the potential [see (3)]. E_0 is the total energy at the minimum of a constant-entropy curve, which can be interpreted as the energy absorbed from the laser. Whereas this interpretation is exact for relatively long laser pulses, which heat Bi adiabatically, the error is never more than ≈5% of E_0, even in the limiting case of an extremely short laser pulse that deposits an energy of $E_0 = 10.5$ mRy/atom, which is the maximum value of E_0 for which our fit is still valid. Therefore, in this paper we have used this interpretation. We wish, however, to stress that it is not complicated to compute corrections to the absorbed laser energy for short pulses using (3).

In summary, we fitted 6468 computed data points to a function with 48 free parameters [28 values of E_0 plus the 20 parameters of (4)–(8)]. Our best-fit parameters are summarized in Table 1. Together with (4)–(8) they give a closed analytical description of the A_{1g} phonon frequency, the quasi-equilibrium value of the atomic coordinate, and the third, fourth, and fifth order anharmonic terms as a function of the energy absorbed from the laser. It is worth mentioning, that the root-mean square of the residuals of our fit was only 0.005 mRy/atom, indicating that our parameterized potential energy surface followed the computed data very closely.

4.4 Time dependence

In [3] we have presented a model for the time dependence of the energy density absorbed from a short laser pulse. The explicit form is given by the sum of expressions (5) and (6) in [3]. This model depends on the following parameters: the

Table 1 Best-fit parameters

Parameter	Fitted value
ν_0	2.98316
ν_1	−0.146079
ν_2	0.0219823
ν_3	−0.00407929
ν_4	0.000370427
ν_5	-1.27975×10^{-5}
z_0	0.234416
z_1	0.00047797
z_2	-3.79899×10^{-6}
z_3	3.51079×10^{-7}
γ_0	−0.698865
$\gamma_{1/2}$	−0.197901
$\gamma_{3/2}$	0.00845577
δ_0	−31.8839
δ_1	0.914822
δ_2	0.16485
δ_3	−0.0103825
ϵ_0	−1.30737
$\epsilon_{1/2}$	1.0219
ϵ_1	−0.176243

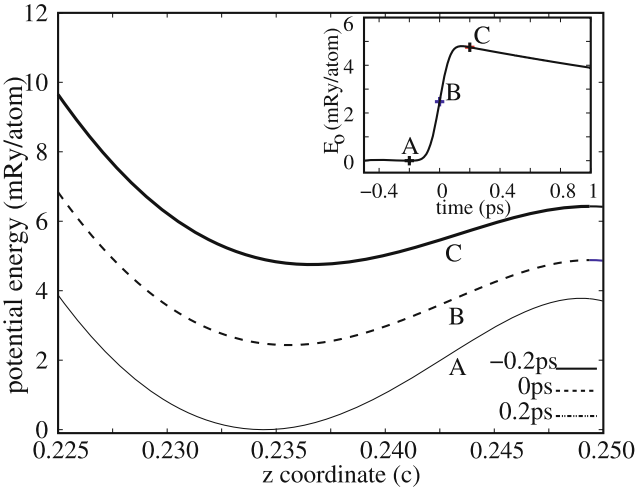

Fig. 2 Computed potential energy at different times during ultrafast laser excitation. The *curves A*, *B*, and *C* correspond to the *points A*, *B*, and *C* in the inset. *A* represents the ground state potential, *B* is the excited potential at the peak time of the Gaussian pulse, and *C* represents the potential at $t = 200$ fs. The *inset* shows the variation of the absorbed energy E_0 as a function of time

electronic energy decay time τ_1, the penetration depth L_0 of the laser light, a diffusion constant D for the electrons and holes, and a constant n_0, which is the total absorbed energy from the laser. Assuming that the optical properties of bismuth do not change during the laser excitation, in the present work, we have simply obtained the time dependence of E_0 for a laser pulse of finite duration by convoluting the model of [3] with the laser pulse shape described below.

In our simulations we have used $\tau_1 = 4$ ps, $D = 0$, $L_0 = 16$ nm, and we have varied n_0. These values are somewhat different from the experimentally determined parameters in [3], but they do not affect our qualitative conclusions of the present paper. To create comparable conditions as in [6] we have assumed that the laser pulse shape is a Gaussian with a full width at half maximum of 130 fs. The resulting time-dependent potential energy surface for $n_0 = 5$ mRy/atom is shown in Fig. 2. We wish to stress that our approach, which combines the model of [3] and the parameterization of Sect. 4.3, can be used to describe the time-dependent potential energy surface of bismuth due to laser pulses of arbitrary shapes and intensities.

5 Quantum simulation of coherent A_{1g} phonons

5.1 Method

In the present work, we assumed that the displacive excitation of coherent phonons (DECP) [20] is the only generating mechanism of the A_{1g} oscillations in Bi (see [7] for a justification of this approximation). The idea behind DECP is that oscillations along the z direction (coherent A_{1g} phonons) are essentially a consequence of the change in the potential equilibrium position z_{eq} due to the laser excitation. When the pulse duration is short enough (approximately less than half a phonon period) to induce such a change nonadiabatically, the atoms start to oscillate about their new equilibrium positions after the laser pulse. Note that our simulations on time-dependent potential energy surfaces automatically include the phonon generation due to DECP.

To describe the evolution of the system on the time-dependent potential of Sect. 4.4, we solved the time-dependent Schrödinger equation

$$i\hbar\frac{\partial\psi(z,t)}{\partial t} = \left[\hat{T} + V(z,t)\right]\psi(z,t). \tag{9}$$

$\hat{T}$ is the kinetic energy operator and $V(z,t) = V(z, E_0(t))$ the potential as given by (3). Please note that the time dependence enters through E_0 as described in Sect. 4.4. ψ is the wave function of the A_{1g} phonons. Because of the complexity of $V(z,t)$, due to the anharmonic terms, we used numerical methods to solve this quantum mechanical equation of motion. First, we constructed two one-dimensional grids, in position and momentum space, where our spatial grid ranged from $z_{min} = 0.227\ c$ to $z_{max} = 0.248\ c$, with 1024 grid points. At low temperature (amplitude collapse and revival in Bi has been observed for $T = 10$ K [6]), only the ground state is occupied. Therefore, a well-defined initial wave packet is formed. This initial state was constructed by solving numerically the time-independent

Schrödinger equation on the spatial grid. We obtained the spatial and time propagation of the quantum wave packet using the split operator technique [21], in which one calculates $\psi(z, t+\delta t)$ from $\psi(z,t)$ by applying the propagator $U(\delta t) \approx e^{-i\delta t V/2} e^{-i\delta t T} e^{-i\delta t V/2}$, where V is evaluated at $t + \delta t/2$. We used an extremely small time step of 0.01 fs, which was necessary to properly account for the time dependence of the Hamiltonian. The potential and kinetic energy operators are diagonal in the position and momentum space, respectively. By going back and forth between our two numerical grids using Fourier transformations the propagator $U(\delta t)$ could efficiently be applied [21].

An important point that we have not addressed so far is how the macroscopic size of bulk bismuth affects the quantum simulations of the A_{1g} phonons. To study this we have introduced a parameter N, which indicates the number of unit cells included in our quantum dynamical simulation. This parameter affects both the initial wave packet and the form of the operators $\hat{V}$ and $\hat{T}$. The case $N = 1$ represents an artificial Bi dimer with exactly the same potential energy surface as bulk bismuth. As this is a finite system, we expected to see clear indications of its quantum nature. To calculate the quantum response of bismuth, we have studied the A_{1g} oscillations as a function of N, where the bulk limit is obtained for $N \to \infty$. Note that, according to our discussion after (1), one expects the emergence of classical mechanics as $N \to \infty$.

5.2 Results

Our computed oscillatory parts of the expectation value of the z coordinate of Bi are shown in Figs. 3 and 4. As pointed out in the previous sections, the oscillations depend on the laser characteristics (fluence, pulse duration, pulse shape). In Fig. 3 we show the dynamics of the phonon wave packet in a two-atom system ($N = 1$). The interaction of the wave packet and the potential leads to a series of collapses and revivals. At low fluences, collapses and revivals are not observed in agreement with experiment [6]. For high fluences, we found that the collapse and revival times increase when the absorbed laser energy is decreased.

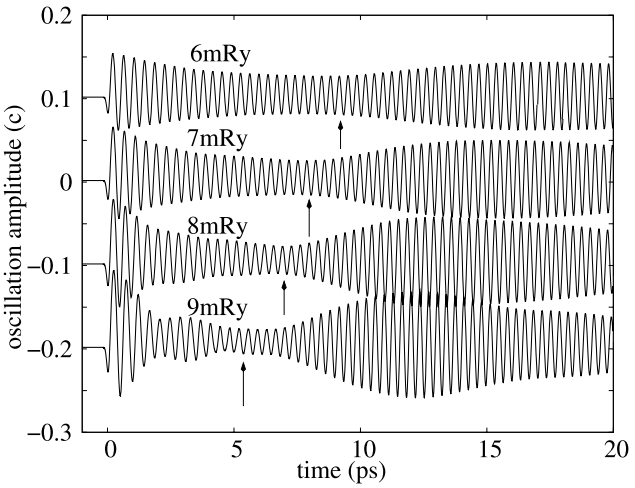

Fig. 3 Oscillatory part of the z coordinate for different absorbed energies n_0. The excitation was caused by a laser with pulse duration of 130 fs. The parameter $N = 1$ (see text). Note that the curves are offset along the y axis, for clarity of presentation. *Arrows* indicate the amplitude collapse of the oscillations

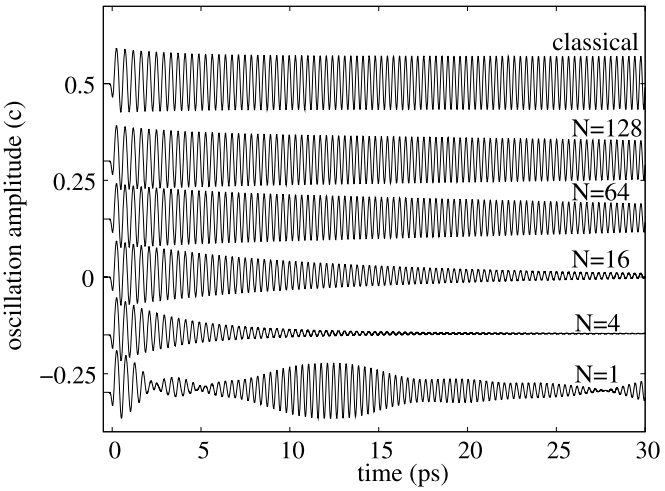

Fig. 4 Oscillatory part of the z coordinate for an absorbed laser energy of $n_0 = 10$ mRy/atom and a pulse duration of 130 fs. *Curves* for different values of N are offset along the y axis. The *five lowest curves* show results from our quantum dynamical simulations and the *uppermost curve* shows the classical trajectory of the resulting A_{1g} oscillation

Figure 4 shows the results of our quantum dynamical simulation as a function of system size. As was to be expected, for large systems the behavior of the quantum system approaches the classical limit (the top curve in Fig. 4). This implicates that the experimentally observed series of beatings in bulk bismuth [6] cannot be explained as a quantum mechanical effect, but is most likely of classical origin.

6 Conclusion and discussion

In this paper we have performed quantum dynamical simulations on time-dependent potential energy surfaces in order to elucidate the origin of experimentally observed [6] beatings of laser-induced coherent phonons in bismuth. By introducing a parameter for the number of unit cells included in our study we found that the behavior of the excited phonons approaches the classical behavior rapidly as a function of system size. This is a strong indication that quantum effects do not play a role in the generation of the observed beatings.

Possible alternative explanations are a classical interference between signals reflected from different parts of the sample or the beating between excited modes of different

symmetries. The first mechanism would presuppose that the sample has been heated unevenly by the laser. Of course from our computations we cannot judge the likeliness of this scenario, but we hope that our study will inspire experimentalists to study this possibility. The second mechanism requires that at least two kinds of phonons are excited in bismuth, that their frequencies are near, and that there is a strong coupling between the two modes. Whereas the first condition is fulfilled (so-called E_g phonons are excited in Bi through Raman scattering), our previous calculations on bismuth [7, 22] indicate that the A_{1g} and E_g frequencies are not close enough to explain the observed beatings and that the coupling between these modes is relatively weak. Therefore, we believe that this latter explanation is unlikely.

Acknowledgements This work has been supported financially by the Deutsche Forschungsgemeinschaft through the priority program SPP 1134 and by the BMBF through the Verbundprojekt FSP301-FLASH (FKZ: 05KS7SJ1).

References

1. S. Hunsche, K. Wienecke, T. Dekorsy, H. Kurz, Phys. Rev. Lett. **75**, 1815 (1995)
2. M. Hase, M. Kitajima, S. Nakashima, K. Mizoguchi, Phys. Rev. Lett. **88**, 067401 (2002)
3. S.L. Johnson, P. Beaud, C.J. Milne, F.S. Krasniqi, E.S. Zijlstra, M.E. Garcia, M. Kaiser, D. Grolimund, R. Abela, G. Ingold, Phys. Rev. Lett. **100**, 155501 (2008)
4. D. Boschetto, E.G. Gamaly, A.V. Rode, B. Luther-Davies, D. Glijer, T. Garl, O. Albert, A. Rousse, J. Etchepare, Phys. Rev. Lett. **100**, 027404 (2008)
5. O.V. Misochko, K. Sakai, S. Nakashima, Phys. Rev. B **61**, 11225 (2000)
6. O.V. Misochko, M. Hase, K. Ishioka, M. Kitajima, Phys. Rev. Lett. **92**, 197401 (2004)
7. E.S. Zijlstra, L.L. Tatarinova, M.E. Garcia, Phys. Rev. B **74**, 220301(R) (2006)
8. I.Sh. Averbukh, N.F. Perelman, Phys. Lett. A **139**, 449 (1989)
9. J.A. Yeazell, M. Mallalieu, C.R. Stroud Jr., Phys. Rev. Lett. **64**, 2007 (1990)
10. M.J.J. Vrakking, D.M. Villeneuve, A. Stolow, Phys. Rev. A **54**, R37 (1996)
11. P. Blaha, K. Schwarz, G.K.H. Madsen, D. Kvasnicka, J. Luitz, *WIEN2k, an Augmented Plane* Wave + Local *Orbitals Program for Calculating Crystal Properties* (Technische Universität Wien, Austria, 2001)
12. P. Hohenberg, W. Kohn, Phys. Rev. **136**, B864 (1964)
13. W. Kohn, L.J. Sham, Phys. Rev. **140**, A1133 (1965)
14. J.P. Perdew, Y. Wang, Phys. Rev. B **45**, 13244 (1992)
15. E. Sjöstedt, L. Nordström, D.J. Singh, Solid State Commun. **114**, 15 (2000)
16. G.K.H. Madsen, P. Blaha, K. Schwarz, E. Sjöstedt, L. Nordström, Phys. Rev. B **64**, 195134 (2001)
17. D. Singh, Phys. Rev. B **43**, 6388 (1991)
18. D.J. Singh, *Planewaves, Pseudopotentials, and the LAPW Method* (Kluwer Academic, Boston, 1994)
19. N.D. Mermin, Phys. Rev. **137**, A1441 (1965)
20. H.J. Zeiger, J. Vidal, T.K. Cheng, E.P. Ippen, G. Dresselhaus, M.S. Dresselhaus, Phys. Rev. B **45**, 768 (1991)
21. M.D. Feit, J.A. Fleck, J. Chem. Phys. **78**, 301 (1982)
22. E.S. Zijlstra, L.L. Tatarinova, M.E. Garcia, Proc. SPIE **6261**, 62610R (2006)